Three-dimensional Image Analysis of Fibrous Materials

Hyunmi Yang[a] and Brent W. Lindquist[b]

[a,b]Department of Applied Mathematics, State University of New York at Stony Brook, Stony Brook, NY 11794-3600

ABSTRACT

A thorough understanding and analysis of geometry and topology of three-dimensional fiber networks from high resolution images is an important and challenging task due to the enormous complexity and randomness of the structure. In this paper we propose a technique that is aimed at structural analysis of fiber mats, both for quality evaluation and improvement of fiber products.

A sequence of image processing techniques is applied to the images, to obtain the medial axis of the fiber network. A description of the network is then determined from the medial axis. We demonstrate computational algorithms that can efficiently identify individual fibers from a network of randomly oriented and curled fibers that are bonded irregularly with each other. We can accurately measure the orientation, location, curl, length, bonds, and crossing angles of the identified fibers as well as the density of the fibers contained in a given volume.

The performance of the proposed technique is presented for simulated fiber data and for a synthetic (polymer) fiber mat.

Keywords: fiber network structure, image processing

1. INTRODUCTION

The main objective of our study is to develop an automated image analysis system that can efficiently identify individual fibers from a three dimensional image of a complex fiber network, and accurately quantify the geometric properties of the network.

Fiber properties such as length, curl, bonds, and orientation distributions are decisive factors of the physical and mechanical properties of fibrous materials. For this reason much effort has gone into developing fiber measurement methods over several decades. Moving from employing microscopy in analyzing fibers (Ref. 1) in 1930's to the development of computerized instruments and imaging systems for automatic measurement of fiber properties (Refs. 2,3) in 1970's was a huge leap in fiber analysis history.

In recent years many researchers have developed image processing techniques to automate the measurement process further. *Xu and Ting*(Ref. 4) suggested an image analysis technique that enables measurements on free fiber segments in thin nonwoven fabrics in a single procedure, using a skeletonization algorithm. *Xu and Ting*(Ref. 5) also explored an application of the Hough transform technique to measure fiber orientation in nonwoven fabrics. In both studies they used $15 \times 15mm^2$ images of fabrics captured through a microscope and a CCD camera. *Pourdeyhimi et al.* suggested chord tracking methods in characterizing fiber orientation in simulated fiber images in Refs. 6,7, and 8. In the above listed research, however, the images of fabrics are taken or assumed to be two dimensional. In dealing with microscopic images, fiber-thickness is not negligible, and hence using a three dimensional volume image of fibrous material will bring a major improvement in the analysis of fibers.

In this paper we report the results of three dimensional analyses on two image data sets, a simulated fiber mat and a real polymer fiber mat. An image of the fiber mat was produced by *synchrotron X-ray computed microtomography*(CAT) (Fig. 1(a)). The simulated data set is $715 \times 715 \times 405$ voxels at 7μ resolution; the real data is $512 \times 512 \times 130$ voxels at 7μ resolution.

Tomographic images are grey scale images and usually contain noise and blurring. In order to identify individual fibers in the image a careful segmentation is necessary. In § 2 we describe two image segmentation methods applied to the data sets.

Further author information:
Hyunmi Yang : hmyang@ams.sunysb.edu
Brent Lindquist: lindquis@ams.sunysb.edu

Applications of Digital Image Processing XXIII, Andrew G. Tescher, Editor,
Proceedings of SPIE Vol. 4115 (2000) © 2000 SPIE · 0277-786X/00/$15.00

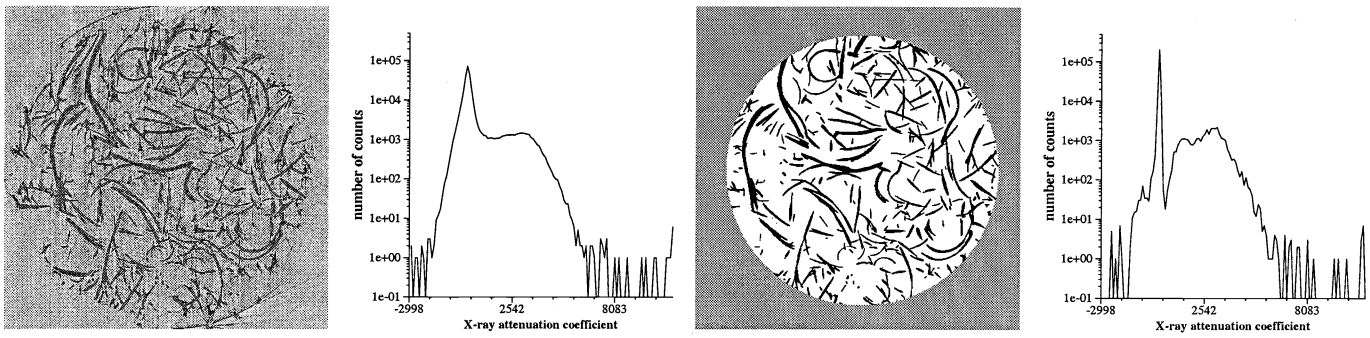

(a) (b) (c) (d)

Figure 1. (a) Raw tomographic image slice of a synthetic fiber data. (b) Segmented image after anisotropic diffusion segmentation. (c) The X-ray attenuation coefficient histogram for the raw data. (d) The attenuation coefficient histogram for the diffused data revealing two sharpened peaks.

A three dimensional fiber network has an extremely complex structure; simplifying the object to its skeleton (medial axis) provides an efficient means for analyzing the network geometry. In § 3 we discuss the medial axis transform method originally suggested by *Lee-Kashyap and Chu*(Ref. 9), and a cluster/path formulation for utilizing the medial axis.

In § 4 we propose a fiber identification algorithm based on the medial axis. In analyzing a fiber network individual fiber identification is the most crucial task. Since fibers touch and curl arbitrarily in random orientation, it is a difficult problem to trace a fiber through the crossings. For this reason, past research on fiber networks has been limited to the *free fiber segments* (segments of fiber having no contact with any other fibers).

Network property results are presented in § 5 for the above mentioned two data sets.

2. IMAGE SEGMENTATION

Three dimensional images of fibrous materials obtained from synchrotron X-ray computed micro-tomography are grey scale images, usually with a bimodal population apparent, each mode corresponding to the void or the fiber space. Segmentation refers to the determination of the phase type of each voxel in the image.

Unfortunately in the serial section images of real set studied here there are large slicewise variations of image intensity. For this reason we segment the real image data set slicewise using the anisotropic diffusion segmentation algorithm suggested by *Perona and Shiota*(Ref. 10). This algorithm assumes that image blurring, which is due to a multitude of causes such as finite spatial resolution and tomographic reconstruction algorithm noise, can be described effectively as the convolution of an original image with a Gaussian kernel and utilizes diffusion to sharpen edges in the convolved image. Typically the histogram of any final diffused image reveals sharpened peaks, and a threshold between the two peaks is chosen. Fig. 1(a) shows one of the image slices of the synthetic polymer fiber mat; its X-ray attenuation histogram is in Fig. 1(b). After performing diffusion, the histogram reveals sharpened peaks as in Fig. 1(d). Choice of an appropriate threshold between the two peaks produces the segmented image in Fig. 1(c).

For the simulated images we employ the kriging-based algorithm of *Oh and Lindquist*(Ref. 11) to perform a fully three dimensional segmentation. The algorithm utilizes indicator kriging based upon estimates of the short length scale spatial covariance of the image.

From the segmented image the porosity/density, *i.e.* the fraction of void/fiber phase volume to total volume, of the image can be computed.

3. MEDIAL AXIS TRANSFORM AND CLUSTER/PATH FORMATION

The medial axis transform is a thinning technique to reduce the dimensionality of a continuum or digitized image of an object, with the goal of providing the inherent geometric 'skeletal' shape of a structure. For an object in continuum space, the medial axis is the union of one-dimensional curve segments, plus possibly surface components

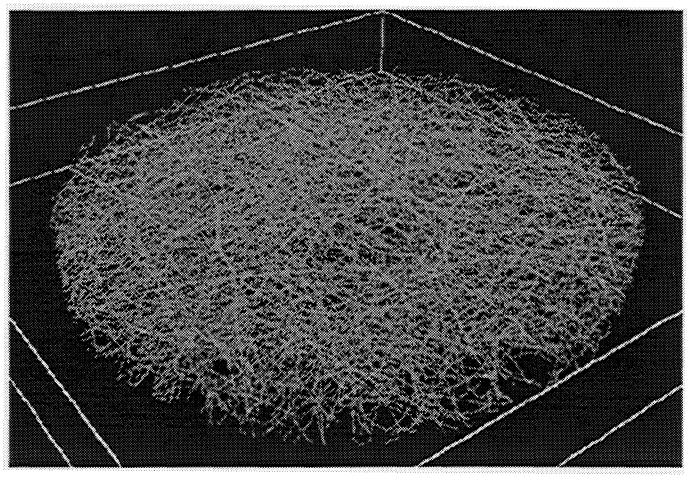

Figure 2. A 3D image of the medial axis of synthetic fiber mat. The color of each voxel represents the closest distance to the fiber surface (burn number).

surrounding embedded cavities. Three or more curve segments join at a **vertex**, and the number of curve segments meeting at the vertex is referred to as the **coordination number** of the vertex.

For a digitized object, the medial axis analog of a curve segment is a **path**, each voxel on a path having exactly two neighbors, with the possible exception of terminating voxels. Since voxels have finite size, the digitized analog of a vertex may consist of several medial axis voxels in order to join a required number of paths. We define a **cluster** as a set of medial axis voxels, each of which has at least three medial axis neighbors that are also in the cluster. Topologically, for the medial axis of a fiber network, clusters are of two types, points and (unions of) circles. We refer to these respectively as **point** and **genus 0 clusters**. A cluster of the second type is shown in Fig. 3(a). Both cluster types serve as digitized representation of vertices which join paths.

For a set of fibers, paths correspond to *free fiber segments*, *i.e.* parts of fibers that do not touch or cross any other fiber, and clusters correspond to fiber-bonds. We utilize a thinning algorithm due to *Lee-Kashyap and Chu*(Ref. 9) with some modifications described in § 4.1. The resultant medial axis for the synthetic polymer network is shown in Fig. 2.

4. FIBER IDENTIFICATION

4.1. Medial axis modification

In order to extract accurate data from the medial axis some modification is appropriate.

Boundary voxel trimming. If fibers exit the imaged region, there is information loss that results in a correct medial axis segment accompanied by a 'pile-up' of incompletely resolved fiber medial axis voxels along the boundary. The boundary trimming algorithm removes all such incompletely resolved boundary voxels, retaining one voxel on the boundary however to document that the fiber exits the boundary.

Path pruning. We classify each path on the medial axis as one of three types: a **branch-branch** path connects to a cluster at each end; a **branch-leaf** path connects to a cluster only at one end; and a **leaf-leaf** path is isolated, having no cluster connection at either end. Leaf-leaf paths arise from disconnected fibers, and correspond to fibers that exit the boundary. As these are incomplete fibers, they are removed from the set.

Construction of the medial axis is sensitive to surface noise in the digitized image. Irregularities in the digitized surface of fibers can mimic dead-end fiber segments, resulting in extra, short, branch-leaf paths on the medial axis. Distinguishing between branch-leaf paths which derive from surface noise and those which derive from genuine fiber ends is difficult. We prune branch-leaf paths whose length is less than a user-specified threshold amount.

Merging close clusters. Consider two fibers which touch, *i.e.* one fiber lies across the other. As fibers have finite thickness, the construction of the fiber medial axis in the vicinity of this region is likely to produce two coordination number 3 branch clusters rather than a single coordination number 4 branch cluster; one very short

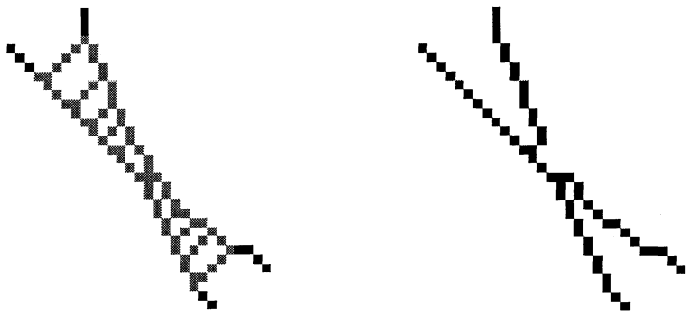

(a) (b)

Figure 3. (a) A 2-D surface remnant formed by two closely lying fibers. Voxels in red represent surface remnant, black represent medial axis path attached to it. (b) After applying surface remnant reduction algorithm, the object is reduced to four medial axis paths joining at the center of mass voxel of the object.

medial axis path will join the two branch clusters. The cluster merge algorithm is designed to merge such 'close' clusters and their joining path to a single branch cluster of coordination number 4, modifying the medial axis. This algorithm requires a user-specified choice of length scale to determine whether clusters are close.

Genus 0 cluster reduction. Fig. 3(a) shows a typical genus 0 cluster (grey voxels). After thinning two fibers which cross at a very acute angle, the resultant digitized medial axis can be 'ladder-shaped'. This is aggravated by cluster merging. The specific topology of a genus 0 cluster is generally irrelevant, our interest is concentrated solely on its location and the paths that connect to it. Therefore, the internal structure of such a cluster can be reduced to retain just the position and connection information in the following manner. From the voxel lying closest to the center of mass of the cluster, the shortest path through the cluster to each attached path is traced. Any cluster voxel not lying on one of these connecting routes is deleted. Fig. 3(b) shows the result of applying this reduction algorithm to the cluster in Fig. 3(a).

4.2. Fiber Tracing Algorithm

Individual fibers bond to each other where they touch (cross). Tracing of individual fibers requires 'joining' paths (free fiber segments) together through clusters to reconstruct the medial axis for a single fiber. Given a branch cluster and the paths that attach to it, this requires associating the paths in pairs, indicating how an individual fiber continues through the branch point.

The following three step algorithm is used to trace individual fibers.

Step 1 : The medial axis path set is examined and all leaf-leaf paths are identified as single fibers.

Step 2: Construct fibers by starting from the leaf-end of a branch-leaf path, and following the **precomputed optimally paired** paths through each cluster reached. The precomputation of optimal pairing through clusters is described below. The fiber will end either at the leaf-end of another branch-leaf path, or at an odd-coordination number cluster. Step two continues until all branch-leaf paths have been assigned to fibers.

Step 3 : After all branch-leaf paths have been used, construct fibers by beginning with the single unpaired path of an odd-coordination number cluster. Continue until no paths remain.

We classify the identified fibers into three groups. **Leaf-leaf** fibers begin and end on a leaf voxel of the medial axis. These fibers are identified in steps 1 and 2 above. **Branch-leaf** fibers begin on a leaf voxel but end at a branch cluster or surface remnants when further continuation of the fiber cannot be done. These fibers are identified in step 2 above. **Branch-branch** fibers begin and end at branch clusters or surface remnants. These fibers are identified in step 3 above.

Optimal path-pairing. The most difficult yet important part in fiber tracing through the network is the pairwise joining of medial axis paths on opposite sides of a branch cluster. We compute the optimal pairs of paths at all clusters before fibers are traced. As fibers bend, it is important to allow for some deviation of angle between the 'incoming' and 'outgoing' fiber paths. For this reason, we employ a minimum kink-angle tolerance θ_{tol} of fibers

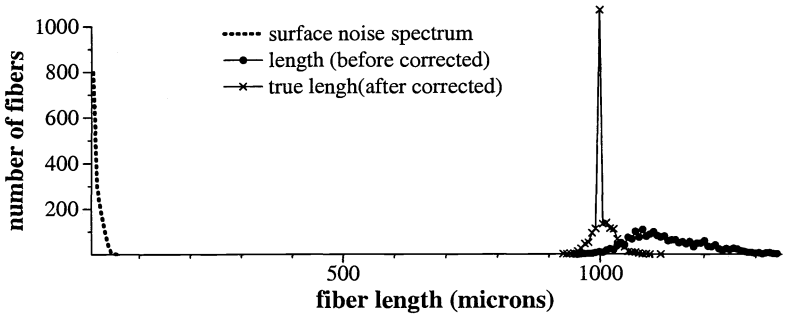

Figure 4. Length distributions of a three dimensional fan of 46^2 fibers of true length 1000μ before and after length correction. Dotted line indicates noise length range.

which may not be exceeded for two paths to be paired. This requires computation of the acute angle of deviation between any two paths that meet at a cluster. As fibers curl, the medial axis paths are not straight lines. For each path, we perform a straight line fit to the centers of the m voxels that lie closest to the cluster and use this straight line fit to determine the deviation angle for the path. The value for m should be less than the total number of voxels on the path.

In addition, linking two paths through a branch cluster to form a fiber also requires finding a voxel path **within the cluster** to use to link the two attached paths. We use the shortest distance route through the network of cluster voxels for this.

4.3. Post Identification Modification

Length correction. Fibers are randomly oriented in space. Consequently, the processes of digitization, segmentation and skeletonization produce a distortion of the measured fiber length distribution. To remedy this, a method of computing length correction factors for each fiber has been developed. The algorithm is designed so that it can be applied not only to straight line fiber data, but also to arbitrarily curved fibers. The procedure is the following.

1) Generate a 3D fan of straight constant length fibers which resemble, in cross sectional shape, the fibers of the network we wish to analyze. The fibers in the fan are arranged in the 3D digitized grid to cover all possible orientations. 2) Perform the segmentation, medial axis transform, and fiber identification on this set of fibers using the same parameters as for the fiber network being studied, and the fibers in the fan are reconstructed. 3)The length distribution of the reconstructed fibers is used to generate a lookup table, referenced by the two angles in a spherical coordinate system. Recorded in each entry of the table is the ratio of the reconstructed fiber length to its input length. For instance, for a fan of 1000μ fibers covering the range 0-45 degrees in each angle, the measured reconstructed lengths vary from 948μ to 1341μ. 4)Since real fibers curve, the lookup table generated from the 3D straight fiber fan cannot be used to correct length measurements taken on whole reconstructed fibers, but rather must be capable of partitioning the fiber into segments, each approximately straight, and using the lookup table to provide correction for each segment in the partition, based upon its spatial reference angles.

Fig. 4 shows a length distribution of a 3D fan of straight fibers of constant length 1000μ showing how true length can be altered in digitized grid.

Filtering of short fibers. Branch-leaf paths on the medial axis due to surface noise effects ultimately end up as very short branch-leaf or leaf-leaf fibers upon fiber tracing. The set of very small fiber segments must be removed from the fiber data set before statistics are collected. A measure of these surface noise generated short fibers can also be determined from the simulated three dimensional fan. The length distribution of the fan of fibers reveals (Fig. 4, dotted line) the presence of these surface noise "fibers" ranging in length from 7 to 63μ. These fibers having length in this range are considered noise and removed.

5. GEOMETRICAL STATISTICS

For the corrected set of identified fibers we provide statistical characterization for the distribution of 1) length, 2) tortuosity, 3) number of bonds, 4) crossing angle, as well as scatter plots on the 5) moments of inertia and principle axes of fibers, which describes their orientation in the three dimensional space. The detailed description of algorithms for measuring each distribution are omitted here.

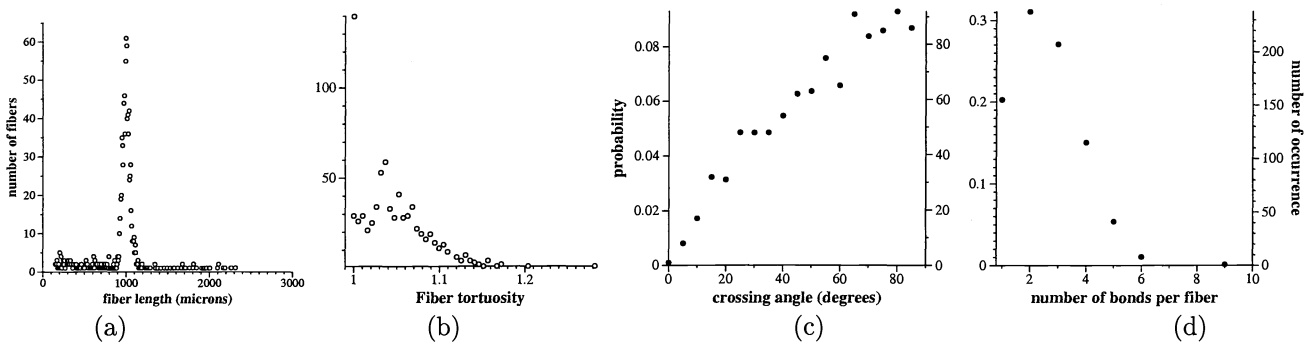

Figure 5. Statistics for the simulated data *SD4* : (a) Fiber length distribution (x-axis is fiber length in μ) . (b) Fiber curl distribution (x-axis is fiber curl). (c) Fiber crossing angle distribution (angle in degrees). (d) Number of bonds per fiber.

Table 1. Summary of distributions for *SD4* and *SYN*.

Distr.		Length	Curl	Crossing angle	Bonds
SD4	Mean	1026.9μ	1.04	55.13	2.58
	SD	31.07μ	0.039	21.50	1.20
SYN	Mean	497.4μ	1.48	53.81	6.06
	SD	285.19μ	0.26	20.82	3.50

5.1. Simulated Fiber Mats

We report the result from a simulated fiber mat. The data set was generated by an industrial mat simulator. It consists of the end point positions of 2984 free fiber segments forming 938 fibers of 40μ thickness and of constant length 1000μ. It is found to have 93% porosity (7% fiber density). The 938 fibers are composed of piecewise straight segments with small bending angles between them. We digitize the data at 7μ voxel resolution, creating a data set of voxel size $715 \times 715 \times 405$, simulating a computed tomographic image. The data is segmented, thinned to produce the fiber medial axis, and modified (§ 4.1) for a fiber tracing (§ 4.2). The fiber identification (§ 4) is followed by noise clean up and length correction as described in § 4.3.

In the fiber length distribution, Fig. 5(a), the peak range (990 to 1116μ) contains 84.7% of the 938 fibers in this data set and has its modal value at the correct length of 1000μ.

Statistics are determined for these fibers only. Fig. 5(b) is the fiber tortuosity (curl) distribution; we find the averge curl of 1.039, which agrees with the original distribution used to generate *SD4*.

Fig. 5(c) shows the crossing angle distribution, ranging from 4.23 degrees to 89.98 degrees measured from 792 fiber crossings. (The crossing angle algorithm finds the smallest of the four angles made by each pair of fibers crossing at a cluster.) The average crossing angle is 57.3 degrees.

Fig. 5(d) is the distribution of number of bonds per fiber. There are 1974 fiber bonds and the average number of bonds per fiber is 2.6. From the bond distribution we obtain an average free fiber segment length 389μ.

Fig. 6 describes the fiber orientation distribution. The top three scatter plots comparing the moments of inertia, demonstrate that short fibers (less than 990μ, in small dots) tend to have smaller *intermediate and large* moments of inertia (consistent with their short length, and that the longer fibers (longer than 1116μ, in cross) tend to have larger moments of inertia in all three directions, consistent with their length and curvature. The second row plots, for each fiber, the principal axis (projected onto the *xy-* *yz-* and *xz*-planes) corresponding to the smallest moment of inertia. The second and the third plots in this row show how the short fibers are often out of the *xy*-plane (mat plane). Rows three and four are the analogous plots for the axes corresponding respectively to the intermediate and large moments of inertia. The distribution for the 84.7% fibers (in circle) is much more realistic.

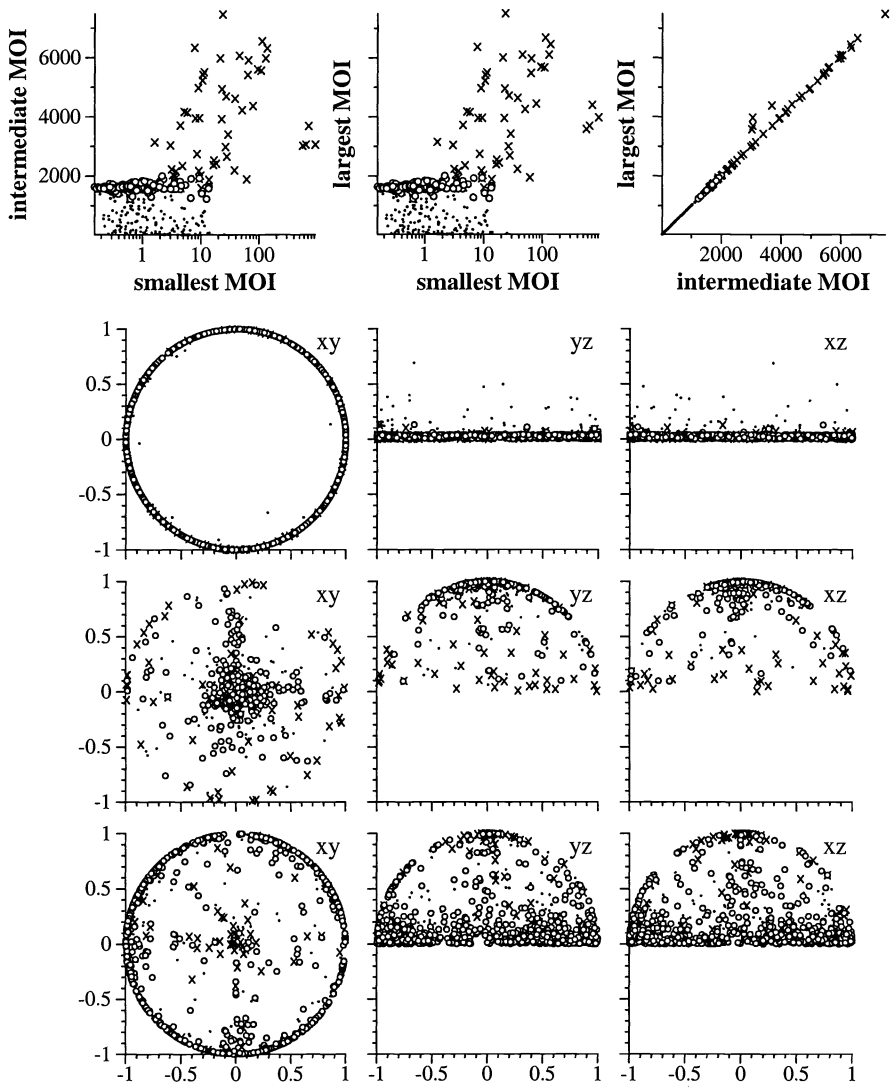

Figure 6. Fiber orientation distribution of all the identified fibers. Marked as circle represent the fibers in correct length range, small dots too short, and x too long. In the bottom three plots only the tips of the projection vectors are plotted.

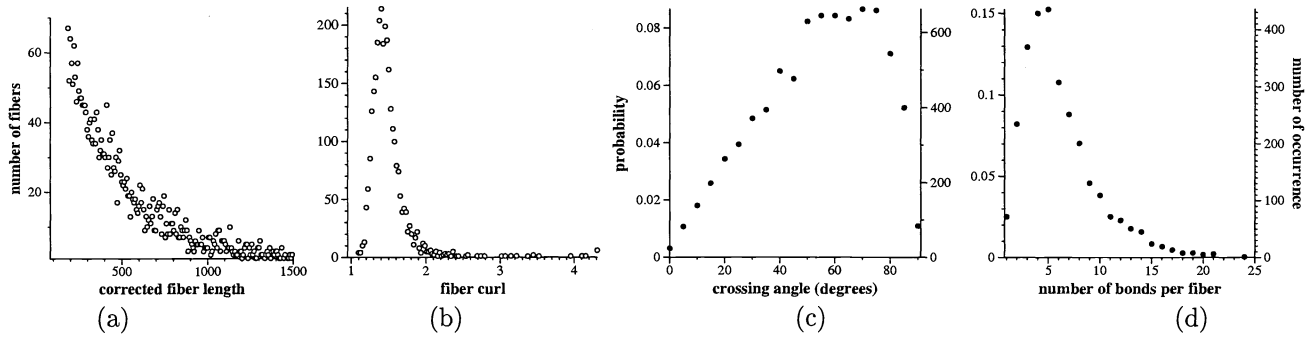

Figure 7. Statistics for the simulated data *SYN* : (a) Fiber length distribution (x-axis is fiber length in μ) . (b) Fiber curl distribution (x-axis is fiber curl). (c) Fiber crossing angle distribution (angle in degrees). (d) Number of bonds per fiber.

Table 2. Summary of CPU times (sec).

	SD4	*SYN*
voxel size	$715 \times 715 \times 405$	$512 \times 512 \times 130$
Segmentation	5727	3818
MA transform	818	105
MA modification	217	3060
Fiber identification /Statistics	10	210

5.2. Real Nonwoven Fiber Mat

SYN is a $512 \times 512 \times 130$ tomographic image of a synthetic fiber mat imaged at 7μ resolution. As shown in Fig. 1(a), the raw tomographic image is noisy. For an efficient segmentation we impose a circular fiducial polygon to border the circular imaged region of fibers. The segmented (§ 2) data is found to have 82% porosity (18% density), and the fiber medial axis is obtained as described in § 3. The resulting medial axis shown in Fig. 2 is extremely complex. The fibers are arbitrarily curled, randomly oriented, the thickness and length of fibers are diverse. Careful medial axis modification is required in deciding the thresholds for *path pruning*, *cluster merge*, and *genus 0 cluster reduction*. Initially there are 15,528 clusters (including 647 genus 0 clusters) and 36,204 paths in the medial axis set. The maximum coordination number of clusters is 46. After modification 13,100 clusters and 25,758 paths are left in the set, and the maximum coordination number is 39.

After the fiber identification step including the fiber modification (§ 4.2), we identify 5424 fibers. We define a length range for successfully identified fibers by using a lookup table that is generated specifically for *SYN*. Fig. 7 shows the distributions obtained from the analysis of *SYN*. The orientation distribution for fibers in *SYN* is omitted in this paper. For this data we report the average fiber length 328.3μ, average curl 1.489, average fiber crossing angle 55.8 degrees, and the average number of bonds per fiber 6.04.

In Table 1 the mean and the standard deviation for the distributions are summarized. In Table 2 the CPU times required for each step on two data sets are reported. It should be noted that all the procedures except for the segmentation of *SYN* were performed on Intel Pentium III Xeon processor. The segmentation for *SYN* was done on IBM RS6000.

REFERENCES

1. F. A. Mennerich, "A rapid microscopical measurement of diameter in cross-section," *Textile Res. J.* **6**, pp. 217–220, 1936.
2. L. J. Lynch and N. A. Michie, "An instrument for the rapid automatic measurement of fiber fineness distribution," *Textile Res. J.* **46**, pp. 653–660, 1976.
3. E. M. Pohle, "Interlaboratory test for wool fineness using the pimc particle measurement computer system," *J. Testing Eval.* **3**, pp. 159–162, 1975.
4. B. Xu and Y. L. Ting, "Measuring structural characteristics of fiber segments in nonwoven fabrics," *Textile Res. J.* **65(1)**, pp. 41–48, 1995.
5. B. Xu and Y. L. Ting, "Determining fiber orientation distribution in nonwovens with hough transform techeniques," *Textile Res. J.* **67(8)**, pp. 563–571, 1997.
6. B. Pourdeyhimi, R. Ramanathan, and R. Dent, "Measuring fiber orientation in nonwovens, part i: Simulation," *Textile Res. J.* **66(11)**, pp. 713–722, 1996.
7. B. Pourdeyhimi, R. Ramanathan, and R. Dent, "Measuring fiber orientation in nonwovens, part ii: Direct tracking," *Textile Res. J.* **66(12)**, pp. 747–753, 1996.
8. B. Pourdeyhimi, R. Dent, A. Jerbi, S. Tanaka, and A. lDeshpande, "Measuring fiber orientation in nonwovens, part v: Real webs," *Textile Res. J.* **69(3)**, pp. 185–192, 1999.
9. T. C. Lee, R. L. Kashyap, and C. N. Chu, "Building skeleton models via 3d medial surface/axis thinning algorithms," *CVGIP: Graph. Models Image Process.* **56**, pp. 462–478, 1994.
10. P. Perona, A. Shiota, and J. Malik, "Anisotropic diffusion," in *Geometry Driven Diffusion in Computer Vision*, B. M. ter Haar Romany, ed., pp. 73–92, Kluwer Academic, Boston, 1994.
11. W. Oh and W. B. Lindquist, "Image thresholding by indicator kriging," *IEEE Trans. Pattern Analysis and Machine Intellegence* **21**, pp. 590–602, 1999.